HHS Public Access

Author manuscript

Int J Radiat Oncol Biol Phys. Author manuscript; available in PMC 2017 December 01.

Published in final edited form as:

Int J Radiat Oncol Biol Phys. 2016 December 01; 96(5): 1078–1086. doi:10.1016/j.ijrobp.2016.08.036.

Simulated Online Adaptive MR-Guided SBRT for the Treatment of Oligometastatic Disease of the Abdomen and Central Thorax: Characterization of Potential Advantages

Lauren Henke, MD, **Rojano Kashani, PhD**, **Deshan Yang, PhD**, **Tianyu Zhao, PhD**, **Olga Green, PhD**, **Lindsey Olsen, PhD**, **Vivian Rodriguez, PhD**, **H. Omar Wooten, PhD**, **H. Harold Li, PhD**, **Yanle Hu, PhD**, **Jeffrey Bradley, MD**, **Clifford Robinson, MD**, **Parag Parikh, MD**, **Jeff Michalski, MD, MBA**, **Sasa Mutic, PhD**, and **Jeffrey Olsen, MD**

Department of Radiation Oncology, Washington University School of Medicine, St. Louis, MO

Abstract

Purpose/Objectives—Stereotactic body radiotherapy (SBRT) is increasingly used to treat oligometastatic or unresectable primary malignancy, although proximity of organs-at-risk (OAR) may limit delivery of sufficiently ablative dose. Magnetic resonance (MR)-based online-adaptive radiotherapy (ART) has potential to improve SBRT's therapeutic ratio. This study characterizes potential advantages of online-adaptive MR-guided SBRT to treat oligometastatic disease of the non-liver abdomen and central thorax.

Materials/Methods—Ten patients treated with RT for unresectable primary or oligometastatic disease of the non-liver abdomen (n=5) or central thorax (n=5) underwent imaging throughout treatment on a clinical MR-IGRT system. SBRT plans were created based on tumor/OAR anatomy at initial CT simulation (P_I) and simulated adaptive plans were created based on observed MR-image set tumor/OAR "anatomy-of-the-day" (P_A). Each P_A was planned under workflow

Corresponding Author: Jeffrey R. Olsen, MD, Department of Radiation Oncology, Washington University School of Medicine, Campus Box 8224, 4921 Parkview Place, Floor LL, St. Louis, MO 63110, (314) 747-2702, (314) 747-5735, (fax), jolsen@radonc.wustl.edu.

Conflict of Interest Statement The authors listed below report the following financial relationships (authors not listed reported no relevant financial relationships):

Dr. Bradley reports departmental funding for clinical trials from ViewRay, and honoraria paid to Washington University by ViewRay for lectures he has given, outside of the submitted work.

Dr. Green reports honoraria from ViewRay, inc, outside the submitted work.

Dr. Henke reports grants from ViewRay Inc, outside the submitted work.

Dr. Jeffrey Olsen reports grants, personal fees and other from ViewRay, Inc, outside the submitted work.

Dr. Lindsey Olsen reports grants from Varian Medical Systems, outside the submitted work.

Dr. Kashani reports grants and personal fees from ViewRay Inc, outside the submitted work.

Dr. Mutic reports grants and other from ViewRay, Inc, grants and other from Varian Medical Systems, other from Philips Healthcare, other from Siemens, other from TreatSafely, LLC, and other from Radialogica, LLC, outside the submitted work.

Dr. Parikh reports grants from Philips Healthcare, grants and other from Varian Medical Systems, other from Holaira, Inc, other from Medtronic/Covidien, outside the submitted work.

Dr. Robinson reports grants and personal fees from Varian, grants from Elekta, personal fees from Radialogica, and personal fees from ViewRay, outside the submitted work;.

Dr. Wooten reports personal fees from ViewRay, Inc, outside the submitted work.

Dr. Yang reports grants from ViewRay and one software license agreement with ViewRay Inc, outside the submitted work.

constraints to simulate online-ART. Prescribed dose was 50Gy/5fractions with goal coverage of 95% PTV by 95% of the prescription, subject to hard OAR constraints. P_I was applied to each MR dataset and compared to P_A to evaluate changes in dose delivered to tumor/OARs, with dose escalation when possible.

Results—Hard OAR constraints were met for all P_I based on anatomy from initial CT simulation, and all P_A based on anatomy from each daily MR-image set. Application of the P_I to anatomy-of-the-day caused OAR constraint violation in 19/30 cases. Adaptive planning increased PTV coverage in 21/30 cases, including 14 cases where hard OAR constraints were violated by the non-adaptive plan. For 9 P_A cases, decreased PTV coverage was required to meet hard OAR constraints that would have been violated in a non-adaptive setting.

Conclusions—Online-adaptive MRI-guided SBRT may allow PTV dose escalation and/or simultaneous OAR sparing compared to non-adaptive SBRT. A prospective clinical trial is underway at our institution to evaluate clinical outcomes of this technique.

Keywords

Online-adaptive radiation therapy; ART; MRI-guided radiation therapy; MR-IGRT; SBRT; Oligometastases; Adaptive Planning

INTRODUCTION

Stereotactic body radiotherapy (SBRT) has emerged as a highly attractive, conformal, and non-invasive means to focally ablate oligometastatic or unresectable primary malignancy (1–3). In-field control rates of metastases treated with SBRT of 80% up to four years after therapy have been reported, including series examining heterogeneous histologies, sites, and dose (4–6). Although many patients who undergo SBRT for oligometastases will experience relapse with distant metastases (DM), approximately 20% of patients with in-field control remain disease-free at 2–4 years follow-up (4, 5, 7). Achievement of disease-free survival (DFS) is contingent upon complete local ablation of metastases (8). For SBRT, improved local control correlates with increased dose, as demonstrated by several dose escalation trials, with reported rates up to 100% at 12 months follow-up (5, 9–11).

Nevertheless, high-dose treatment of oligometastatic/unresectable primary disease with SBRT has been historically limited by normal tissue toxicity. This narrow therapeutic ratio is most evident in the central thorax, where attempted dose-escalated treatment of tumors proximal to critical structures of the mediastinum has caused pronounced increase in unacceptable toxicity, and in the abdomen, where proximity to radiosensitive organs including bowel and attempts to account for respiratory motion may increase toxicity and limit dose (12, 13).

The safe ablation of oligometastatic or unresectable primary disease with SBRT depends on accurate target delineation and localization. Until recently, technology to define and track targets during treatment has been limited to either internal tumor surrogates such as fiducial markers, or external tumor surrogates including patient surface anatomy for correlation with internal motion. These modalities may inadequately account for intrafractional organ motion and do not address interfractional motion or variability in the position of organs-at-risk

(OARs), which remain significant sources of positional uncertainty (14–18). In contrast to CT-based imaging for daily setup, onboard low-field MRI may improve soft tissue visualization for accurate definition of target volumes (19).

Recently, the necessary technology and treatment planning system (TPS) for implementation of online-ART was developed in the form of a dedicated MR-image-guided radiotherapy (MR-IGRT) system (20–23). With respect to SBRT, daily reoptimization of treatment plans based on observed daily anatomy could provide the accurate real-time target delineation that is essential for OAR sparing and dose escalation. However, potential improvements in the therapeutic ratio of SBRT using online-ART have yet to be evaluated in the context of clinical implementation of new MR-IGRT technology.

To evaluate potential applications of ART for SBRT, we compare CT-based, non-adaptive SBRT plans with simulated MR-IGRT-based adaptive plans. In this study, we characterize the potential advantages of online-adaptive MR-guided SBRT to treat oligometastatic or unresectable primary disease of the abdomen and central thorax. We hypothesized that compared with CT-based non-adaptive SBRT, simulated online-adaptive MR-guided SBRT planning may reduce OAR dose and potential toxicity while allowing dose escalation.

METHODS AND MATERIALS

Patient and tumor characteristics

Ten patients treated at our institution from 2014–2015 with CT-simulated, non-adaptive radiation therapy for unresectable primary/oligometastatic disease of the central thorax or abdomen were identified for inclusion in this study. Patient and tumor characteristics are listed in Table 1. Initial clinical treatment, consisting of fractionated therapy (n=3) or SBRT (n=7), occurred either on a linear accelerator-based system (n=3) or an MR-IGRT-Co-60-based system (n=7). All patients, including those not clinically treated with SBRT, had disease limited to 1–2 oligometastatic/unresectable primary lesions that were retrospectively deemed appropriate for online-adaptive SBRT, had such technology been available at time of treatment. For patients treated on the MR-IGRT system, localization images were used for adaptive stereotactic replanning in this study. Patients not treated with MR-IGRT were selected based on prior inclusion on a separate, MR imaging study, in which they underwent additional daily imaging throughout treatment on a clinical MR-IGRT system.

Treatment system; time and workflow constraints

All initial and adaptive planning was performed using a dedicated MR-IGRT TPS (ViewRay Inc. Oakwood Village, OH) under time/workflow constraints to simulate online-ART. This clinical workflow has been previously described (24). In brief, the clinically-deployed, MR-IGRT unit comprises a split-solenoid 0.35 Tesla MR scanner mounted on a ring gantry with three MLC-equipped ^{60}Co heads. On each treatment day, a high-resolution volumetric MR-image (1.5x1.5x3.0mm isotropic for all patients included in this study) is acquired for each patient at time of setup. Deformable registration is performed using the planning CT dataset, followed by transfer of contours and electron density map to the daily MR. All contours were confirmed by a physician and edited manually when needed. The deformed electron

density map is then used to recalculate dose of the original plan on the daily MR for physician evaluation. The supporting Monte Carlo-based TPS is accessible from the delivery workflow, permitting real-time adaptive planning while the patient is on the table. TPS details have been previously described (22). For this study, all imaging data was prospectively collected, but dose recalculation and adaptive planning were retrospectively performed.

Initial, non-adaptive planning

Traditional, non-adaptive SBRT plans were retrospectively simulated for all patients, regardless of prior treatment modality, based on tumor/OAR anatomy at initial CT-simulation (P_I). Clinical simulation for thoracic patients included a free-breathing helical CT scan used for planning for this study. For abdominal patients, CT simulation was at exhale-breath hold. The hypothetically prescribed dose was 50Gy/5 fractions with goal coverage of 95% of the planned target volume (PTV) by 95% of prescription dose. PTV coverage was subject to hard OAR constraints (Table 2). Constraints were selected based on current SBRT institutional practice for thoracic and abdominal treatment sites. When necessary, dose de-escalation to the PTV was performed in order to meet hard constraints with the goal of toxicity avoidance, in accordance with a strict isotoxicity approach.

Simulated adaptive planning

Additional daily, simulated adaptive plans (P_A) were then created based on variable tumor/OAR anatomy observed on each of three subsequent MR-image sets. These MR-image sets were obtained on each patient's actual SBRT treatment days to accurately capture daily anatomic variation. All daily MR-images were prospectively obtained at free-breathing for thoracic patients and exhale-breath hold for abdominal patients. Virtual dosimetric re-planning was then performed to simulate adaptive planning, using a single breath-hold MR-image for formation of P_A. If target coverage or OAR dose exceeded constraints (Table 2), re-optimization was performed using original beam angles and optimization objectives. Additionally, in cases where hard OAR constraints required dose de-escalation at expense of PTV coverage in P_I, PTV dose escalation to a maximum of 60Gy was performed in P_A if more favorable daily OAR anatomy was observed. Dose escalation was based on this maximum prescription dose, applied on a fraction-by-fraction basis (maximum of 12Gy per fraction) to avoid excess dose to an OAR in any individual treatment fraction. Each adaptive fraction was planned and evaluated using a target dose and OAR constraints that were scaled to 5 fractions, without dose accumulation. An adaptive plan was deemed acceptable when OAR constraint compliance was met, with a secondary objective of maximized PTV coverage/dose. For all patients, three P_A were constructed for comparison to P_I.

We then evaluated changes in dose delivered to tumors and OARs between traditional, non-adaptive P_I and all subsequent P_A. To do so, P_I was applied to each daily MR contour and dataset. Specifically, virtual couch correction was used for virtual patient set up to the PTV itself, with subsequent P_I application by study physicians to achieve maximal three-dimensional overlap between the PTV from time of the simulation and the actual observed daily MR target anatomy. Dose for P_I was recalculated on the observed "anatomy of the day" via transfer of the electron density map from the initial CT simulation dataset to the

daily MR with deformable registration. Recalculated P_I dose was then compared to the corresponding daily P_A using side-by-side comparison of isodose distributions and dose volume histograms (DVH). Any changes in dose delivered to tumors/OARs between P_I and P_A were recorded.

Evaluation parameters

Specific changes in dose recorded included 95% PTV coverage, increase or decrease in PTV coverage with adaptive plans relative to the initial plan, violation of mean dose constraints for OARs, and the frequency and extent of violation of maximum dose to OARs according to predetermined constraints (Table 2). Frequency and extent of dose constraint violations and 95% PTV coverage were compared between P_I and P_A.

RESULTS

Organ-at-risk constraints

A total of 30 P_A were constructed. Hard OAR constraints were met for all P_I based on anatomy from initial CT simulation. Similarly, all P_A met hard OAR constraints based on anatomy-of-the-day from each daily MR-image set. Significant interfractional variation was observed in relationships between tumor and OAR anatomy. Figure 1 demonstrates the observed degree of interfractional shifts in the position of OARs relative to target volumes when simulation anatomy was compared to daily treatment anatomy (Fig. 1a versus 1b), and when daily treatment anatomy was compared to subsequent daily treatment anatomy (Fig. 1b versus 1c). Although all initial plans based on simulation anatomy adhered to the OAR constraints (represented by Figure 2a), when these P_I were subsequently applied to the treatment day anatomy captured by each MR-image set, violation of hard OAR constraints occurred in 19/30 cases (represented by Fig 2b). All patients had ≥ 1 fraction with ≥1 OAR constraint violation when P_I was applied to daily MR anatomy. By contrast, potential OAR violations were resolved by adaptive planning (representative example, Fig 2c), resulting in 0/30 P_A OAR violations.

For thoracic cases, common OAR violations for application of P_I to daily anatomy included the trachea (n=6) and esophagus (n=5). For abdominal cases, the most common OARs to receive excess dose via traditional non-adaptive planning were the duodenum (n=7) and stomach (n=6). Figure 2 illustrates a representative duodenal dose violation and subsequent resolution with adaptive planning. OAR violations were variable, both in terms of volume of OARs that received excess dose (Table 2) and magnitude by which constraints were exceeded (Figure 3). For example, when the duodenal dose constraint of 0.5cc ≤ 35Gy was exceeded, the range of duodenal volume treated to ≥35Gy was 0.9cc-12.85cc (mean 8.3cc, median 5.8cc), with maximum dose to the 0.5cc constraint volume ranging from 35.7Gy-46.6Gy. A complete summary of OAR violation type and magnitude is represented in Table 2 and Figure 3.

Target volume coverage

Increased PTV coverage was achieved by adaptive planning in 21/30 fractions. Dose was increased in 10/15 (66.7%) of abdominal and 11/15 (73.3%) of thoracic fractions. PTV dose

escalation relative to the initial plan occurred concurrently with reversal of ≥1 OAR violation in 14/21 (66%) of cases where hard OAR constraints were initially violated by application of P_I to the anatomy-of-the-day. Specifically, improved PTV dose coverage was possible despite increased OAR protection in 7/11 (63%) dose-escalated thorax fractions and 8/10 (80%) dose-escalated abdominal fractions (example DVH, Figure 4a). For nine P_A cases, decreased PTV coverage relative to P_I was required to meet hard OAR constraints that would have otherwise been violated in a non-adaptive setting (example DVH, Figure 4b). When no OAR violation occurred by application of P_I to the anatomy-of-the-day, PTV dose was increased in 9/9 (100%) of fractions. Goal 95% PTV coverage by 47.5Gy (95% prescription dose) was met in 7/30 P_I and 13/30 P_A. Average PTV coverage (all fractions included) for thorax cases was 88.1% at the 95% isodose line for P_I and 92.4% at the 95% isodose line for P_A. For non-liver abdomen cases planned to 50Gy, only 70.7% of the PTV was covered at the 95% isodose line by P_I, with improvement to 83.4% PTV coverage, on average, by P_A. Overall, when PTV dose escalation was achievable, median dose increase (relative percentages of the initial dose covering 95% of the PTV) was 11.2% (range 2.2–52.9%).

DISCUSSION

We present a dosimetric analysis of potential benefits of online-adaptive MRI-guided SBRT for treatment of oligometastatic/unresectable primary disease in the central thorax and abdomen. Application of SBRT as an ablative therapy may be limited in these sites by positional uncertainty and toxicity risk. We hypothesized that online-adaptive MRI-guided SBRT might allow PTV dose escalation and/or simultaneous OAR sparing when compared to non-adaptive SBRT, and confirmed this using simulated online-adaptive planning for 10 patients under workflow and time constraints similar to our clinical MR-IGRT implementation.

Application of traditional SBRT plans to the observed daily MR anatomy resulted in numerous unplanned, potentially toxic violations of dose constraints for organs-at-risk (Figure 2b). Notably, every patient in this study had at least one normal tissue constraint violation in at least one non-adaptive fraction. Although constraint violation magnitude was variable and it is possible that low-level violations would not have resulted in clinically meaningful normal tissue toxicity, several patients' OAR doses markedly exceeded the permitted limit (Table 2, Fig. 3). It is plausible that cases with substantial variability in OAR position and delivered dose may represent the subset of patients who experienced high-grade toxicity in prior SBRT dose escalation trials—such as those observed by Timmerman et al. in the central thorax (12).

Despite high frequency of OAR constraint violations in non-adaptive fractions (61%), we demonstrated successful resolution of violations in all cases by online-adaptive planning. Resolution of normal tissue constraint violation was equally achievable in the abdomen and central thorax. Online-adaptive planning may allow daily identification of this variability, and provide opportunity to eliminate unanticipated toxicity and safely deliver dose-escalated therapy. Further data regarding clinical outcomes is required.

We also observed that adaptive planning allowed PTV dose increase relative to initial plans in a majority of patients and treatment fractions, including those where OAR violations were present following application of the initial plan. Given that our goal of coverage of 95% of the PTV at 47.5Gy (95% of prescription) is typically higher than OAR constraints that would be used in treatment sites such as the abdomen, sacrifice of PTV coverage was often necessary in initial planning due to prioritization of OAR protection. Of note, our median simulated hotspot was 120% of 50Gy (range 109–130%); we chose to limit excessive hotspots because of concerns regarding potential toxicity risk, in the context of dose-escalated treatment. However, our findings suggest that online-ART may permit improved PTV dose coverage on a fraction-by-fraction basis for patients whose simulation anatomy requires a conservative plan. In fact, for most (66%) simulated fractions where adaptive planning was required for OAR protection, simultaneous dose escalation toward/beyond goal prescription of 50Gy was achievable. Dose escalation was also achieved by P_A in 100% of patients whose daily anatomy was favorable and did not result in OAR violation by P_I. The clinical benefits achieved by such dose escalation using this technique require future study. However, for oligometastases, disease control has been demonstrated to increase with increasing dose, approaching 100% with appropriate dose escalation (5, 9–11). Our findings indicate that MR-guided online-adaptive planning could improve local control of oligometastatic disease without increasing toxicity.

Our findings are encouraging to inform potential clinical applications of online-adaptive, MR-guided SBRT. Although the prospective dosimetric and clinical feasibility of MR-guided SBRT planning and treatment have recently been demonstrated, feasibility and clinical applicability of online-adaptive planning has yet to be confirmed (25, 26). While online-adaptive planning was retrospectively simulated in this study, the process used was similar to that implemented as part of our clinical workflow, with MR imaging data that was prospectively collected. This allowed us to represent interfractional target volume motion and potential advantages of online-ART with maximum accuracy. It is possible that the impact and limitations of five-fraction OAR constraints would be partially ameliorated with use of a less-hypofractionated treatment regimen. Similarly, use of greater hotspots potentially can result in steeper dose fall-off in immediate proximity to the target. However, the principle of variable daily OAR anatomy still applies, as does the challenge of treating tumors adjacent to critical OARs (27). Similarly, calculation of true dose accumulation to organs-at-risk is not presently available with our treatment planning process. We recognize that the absence of dose accumulation in the context of an isotoxicity dose escalation approach may cause overestimation of the impact of observed changes in anatomy on OAR dose. Although dose deformation and accumulation is of future research interest at our institution, we have clinically implemented the isotoxicity approach presented here, recognizing it as a conservative approach in order to minimize complication risk. Additionally, we recognize as a limitation that some observed differences in anatomy from simulation to time of treatment in this study may be attributable to differences in CT versus MR-image set data. However, given that very high-dose fractions of radiation are delivered with SBRT, even small changes in daily anatomy risk significant underdosage of portions of the tumor by up to 20% and inadvertent overdose of OARs, creating risk of patient injury. Importantly, significant interfractional motion was also demonstrated between sequential

MR datasets (Fig 1). These findings are consistent with previous reports of interfractional organ motion and deformation where imaging modality remained consistent both from time of simulation to time of treatment delivery and between fractions(20). Given limitations of comparison across image modalities, MR-only planning is of future interest to minimize this potential bias. Finally, although ART may require additional time for physicians, physicists, therapists, and patients, our institution has implemented online-adaptive IMRT planning within an acceptable clinical time frame (median institutional time of 26 minutes for re-contouring, reoptimization, and QA) (24). Our online-adaptive workflow for IMRT is identical to that used for online-adaptive SBRT, and thus online-adaptive SBRT should be similarly feasible. Overall, we demonstrate here that online-adaptive SBRT is likely to achieve significant dosimetric gains. However, prospective evaluation of online-ART is needed for dosimetric validation, to evaluate time required to deliver online-ART in real-time, and to evaluate if dosimetric gains translate into clinical benefit.

Future directions include the ongoing clinical implementation of real-time, online-adaptive MR-guided SBRT at our institution (28) and MR-only treatment planning. Based on this encouraging dosimetric study, we opened a prospective study evaluating use of this technique to treat oligometastatic or unresectable primary disease of the abdomen and central thorax. Data collected will be used to evaluate a primary endpoint of clinical feasibility/timing, with secondary endpoints including tumor response rate, survival, and quality of life metrics.

References

1. Potters L, Kavanagh B, Galvin JM, et al. American Society for Therapeutic Radiology and Oncology (ASTRO) and American College of Radiology (ACR) practice guideline for the performance of stereotactic body radiation therapy. Int J Radiat Oncol Biol Phys. 2010; 76:326–332. [PubMed: 20117285]
2. Timmerman RD, Kavanagh BD. Stereotactic body radiation therapy. Curr Probl Cancer. 2005; 29:120–157. [PubMed: 16059851]
3. Timmerman RD, Kavanagh BD, Cho LC, et al. Stereotactic body radiation therapy in multiple organ sites. J Clin Oncol. 2007; 25:947–952. [PubMed: 17350943]
4. Milano MT, Katz AW, Muhs AG, et al. A prospective pilot study of curative-intent stereotactic body radiation therapy in patients with 5 or fewer oligometastatic lesions. Cancer. 2008; 112:650–658. [PubMed: 18072260]
5. Salama JK, Hasselle MD, Chmura SJ, et al. Stereotactic body radiotherapy for multisite extracranial oligometastases: final report of a dose escalation trial in patients with 1 to 5 sites of metastatic disease. Cancer. 2012; 118:2962–2970. [PubMed: 22020702]
6. Inoue T, Katoh N, Aoyama H, et al. Clinical outcomes of stereotactic brain and/or body radiotherapy for patients with oligometastatic lesions. Jpn J Clin Oncol. 2010; 40:788–794. [PubMed: 20406944]
7. Kang J-K, Kim M-S, Kim JH, et al. Oligometastases confined one organ from colorectal cancer treated by SBRT. Clin Exp Metastasis. 2010; 27:273–278. [PubMed: 20373133]
8. Pastorino U, Buyse M, Friedel G, et al. Long-term results of lung metastasectomy: prognostic analyses based on 5206 cases. J Thorac Cardiovasc Surg. 1997; 113:37–49. [PubMed: 9011700]
9. Herfarth KK, Debus J, Lohr F, et al. Stereotactic single-dose radiation therapy of liver tumors: results of a phase I/II trial. J Clin Oncol. 2001; 19:164–170. [PubMed: 11134209]
10. Wulf J, Baier K, Mueller G, et al. Dose-response in stereotactic irradiation of lung tumors. Radiother Oncol. 2005; 77:83–87. [PubMed: 16209896]

11. Timmerman R, Papiez L, McGarry R. Extracranial stereotactic radioablationresults of a phase I study in medically inoperable stage I non-small cell lung cancer. Chest. 2003; 124:1946–1955. [PubMed: 14605072]
12. Timmerman R, McGarry R, Yiannoutsos C, et al. Excessive toxicity when treating central tumors in a phase II study of stereotactic body radiation therapy for medically inoperable early-stage lung cancer. J Clin Oncol. 2006; 24:4833–4839. [PubMed: 17050868]
13. Hoyer M, Roed H, Traberg Hansen A, et al. Phase II study on stereotactic body radiotherapy of colorectal metastases. Acta Oncol. 2006; 45:823–830. [PubMed: 16982546]
14. James SS, Mishra P, Hacker F, et al. Quantifying ITV instabilities arising from 4DCT: a simulation study using patient data. Phys Med Biol. 2012; 57:L1–L7. [PubMed: 22343122]
15. Ge J, Santanam L, Yang D, et al. Accuracy and consistency of respiratory gating in abdominal cancer patients. Int J Radiat Oncol Biol Phys. 2013; 85:854–861. [PubMed: 22717241]
16. Ge J, Santanam L, Noel C, et al. Planning 4-Dimensional Computed Tomography (4DCT) Cannot Adequately Represent Daily Intrafractional Motion of Abdominal Tumors. Int J Radiat Oncol Biol Phys. 2013; 85:999–1005. [PubMed: 23102840]
17. Shah C, Grills IS, Kestin LL, et al. Intrafraction variation of mean tumor position during image-guided hypofractionated stereotactic body radiotherapy for lung cancer. Int J Radiat Oncol Biol Phys. 2012; 82:1636–1641. [PubMed: 21489715]
18. Cai J, McLawhorn R, Read PW, et al. Effects of breathing variation on gating window internal target volume in respiratory gated radiation therapy. Med Phys. 2010; 37:3927–3934. [PubMed: 20879555]
19. Noel CE, Parikh PJ, Spencer CR, et al. Comparison of onboard low-field magnetic resonance imaging versus onboard computed tomography for anatomy visualization in radiotherapy. Acta Oncol. 2015:1–9.
20. Liu F, Erickson B, Peng C, et al. Characterization and Management of Interfractional Anatomic Changes for Pancreatic Cancer Radiotherapy. Int J Radiat Oncol Biol Phys. 2012; 83:e423–e429. [PubMed: 22436785]
21. Mutic S, Dempsey JF. The ViewRay system: magnetic resonance-guided and controlled radiotherapy. Semin Radiat Oncol. 2014; 24:196–199. [PubMed: 24931092]
22. Wooten HO, Green O, Yang M, et al. Quality of Intensity Modulated Radiation Therapy Treatment Plans Using a ^{60}Co Magnetic Resonance Image Guidance Radiation Therapy System. Int J Radiat Oncol Biol Phys. 2015; 92:771–778. [PubMed: 26104932]
23. Li HH, Rodriguez VL, Green OL, et al. Patient-specific quality assurance for the delivery of (60)Co intensity modulated radiation therapy subject to a 0.35-T lateral magnetic field. Int J Radiat Oncol Biol Phys. 2015; 91:65–72. [PubMed: 25442343]
24. Acharya S, Fischer-Valuck BW, Kashani R, et al. Online Magnetic Resonance Image Guided Adaptive Radiation Therapy: First Clinical Applications. Int J Radiat Oncol Biol Phys. 2016; 94:394–403. [PubMed: 26678659]
25. Kishan AU, Cao M, Mikaeilian AG, et al. Dosimetric feasibility of magnetic resonance imaging-guided tri-cobalt 60 preoperative intensity modulated radiation therapy for soft tissue sarcomas of the extremity. Practical Radiation Oncology. 2015; 5:350–356. [PubMed: 25749215]
26. Kishan AU, Cao M, Wang P-C, et al. Feasibility of magnetic resonance imaging-guided liver stereotactic body radiation therapy: A comparison between modulated tri-cobalt-60 teletherapy and linear accelerator-based intensity modulated radiation therapy. Practical Radiation Oncology. 2015; 5:330–337. [PubMed: 25823383]
27. Li Q, Swanick CW, Allen PK, et al. Stereotactic ablative radiotherapy (SABR) using 70 Gy in 10 fractions for non-small cell lung cancer: exploration of clinical indications. Radiother Oncol. 2014; 112:256–261. [PubMed: 25108807]
28. Olsen, JR., Henke, LE., Kashani, R., et al. Adaptive MRI-Guided SBRT for Unresectable Primary or Oligometastatic Central Thorax and Abdominal Malignancies. 2015. httpsclinicaltrials.govctshowNCT

Summary

In this study, potential dosimetric gains from daily online adaptive SBRT for central thoracic and abdominal applications were characterized. Initial CT-simulation plans were applied to MR localization images, with evaluation and reoptimization based on variable anatomy. We found a significant incidence of OAR constraint violation by application of the initial plan to localization images. Online adaptive planning resolved all potential OAR violations, and allowed dose escalation in a majority of patients and fractions. Our findings suggest that this method could improve the therapeutic ratio for SBRT of central thoracic and abdominal malignancies.

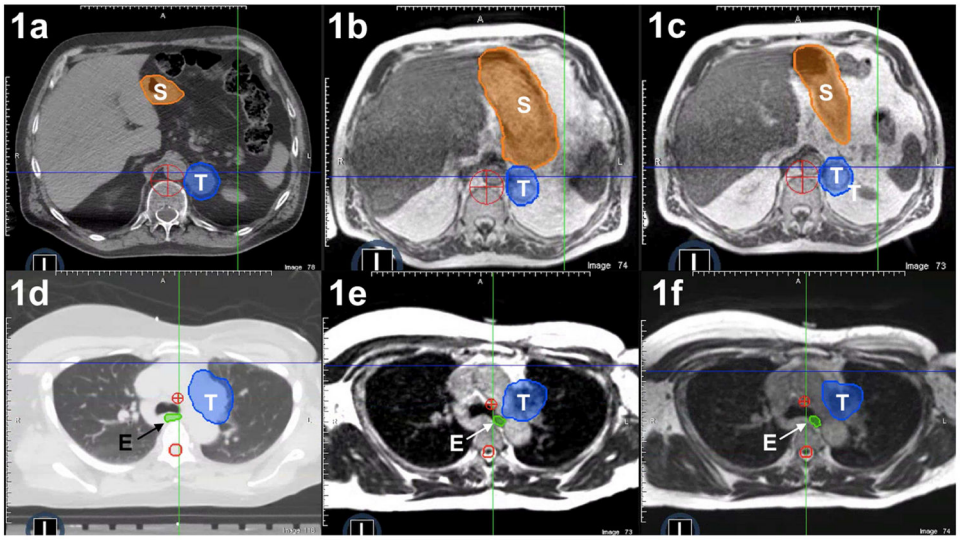

Figure 1.

Patient anatomy at simulation (1a, 1d) compared with “anatomy-of-the-day” revealed by the MR-image set at fraction one (1b, 1e) versus “anatomy-of-the-day” revealed by MR imaging at fraction two (1c, 1f). In frames 1a–1c, large interfractional shifts occur in the position of the stomach (S) relative to the adrenal tumor (T). Similarly, in a separate patient (frames 1d to 1f), interfractional variability in esophageal position (E) relative to a paraaortic lymph node tumor (T) was observed.

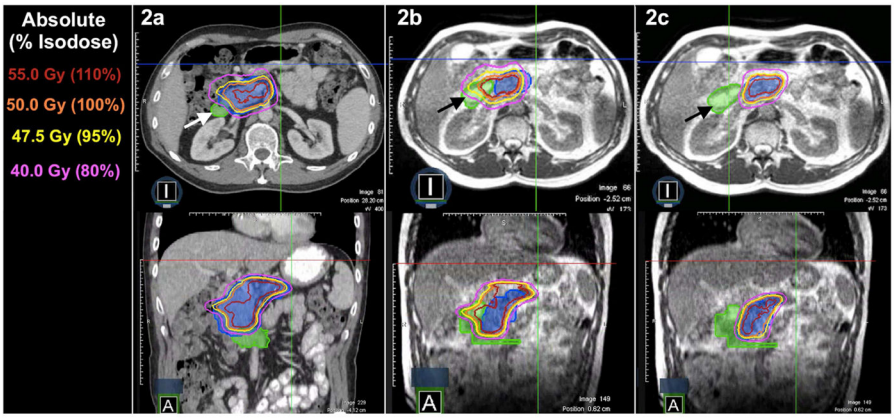

Figure 2.

Computed tomography (CT)-based, non-adaptive P_I met all organ-at-risk (OAR) constraints based on anatomy from initial CT simulation (2a). Application of P_I to the daily MR-image set of a patient with a pancreatic tumor (blue colorwash) resulted in violation of hard duodenal constraints (2b). Daily adaptive planning achieved resolution of the OAR constraint violation to the duodenum (marked with arrows) while preserving target volume coverage (2c).

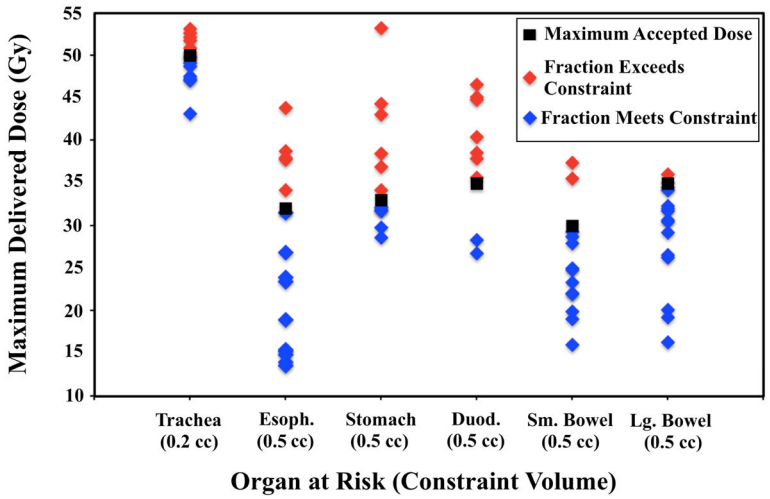

Figure 3.

Maximum point dose delivered to constraint volumes of organs-at risk (OARs) when initial non-adaptive plans were applied to daily anatomy.

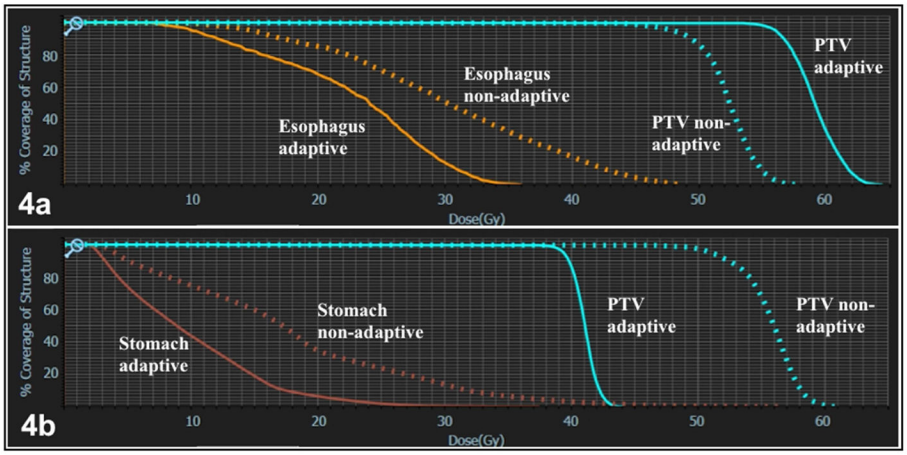

Figure 4.

Dose-volume histograms (DVH) comparing esophageal (4a), stomach (4b), and planning target volume (PTV, 4a and 4b) dose for initial simulation plans based on simulation anatomy, non-adaptive plans applied to daily anatomy, and daily adaptive plans. In 4a, esophageal protection occurred concurrently with PTV dose escalation. In 4b, dose de-escalation to the PTV was required to meet hard stomach constraints.

Table 1

Patient and tumor characteristics

Disease site	
Central thorax	5
Inoperable hilar non-small cell lung cancer	2
Mediastinal lymph node	2
Peri-hilar lymph node	1
Abdomen	5
Adrenal mass	1
Extra-hepatic cholangiocarcinoma	1
Internal iliac lymph node	1
Inoperable pancreas adenocarcinoma	2
Median age (range)	70 (48–81)
Median tumor size in cm (range)	3.4 (0.8–8.0)

Table 2

Hard Dose Constraints for Initial and Adaptive Plans, with Recorded Organ-at-risk Violation Metrics for Application of Non-adaptive Plans (P_I) to MR Localization Images

			Degree of Violation						Degree of Violation		
Abdominal OAR	**Constraint**	**# of PI constraint violations**	**Mean (Std Dev)**	**Median**	**Range**	**Thorax OAR**	**Constraint**	**# of PI constraint violations**	**Mean (Std Dev)**	**Median**	**Range**
Uninvolved liver (liver - GTV)	700cc < 20 Gy	1	NA	NA	NA	Lungs (combined)	V12.5Gy ≤ 1500 cc	0	NA	NA	NA
	V25Gy < 33%	0	NA	NA	NA		V13.5Gy ≤1000 cc	0	NA	NA	NA
	Mean < 20 Gy	1	1 Gy	1 Gy	1 Gy	Esophagus max	V32Gy ≤ 0.5 cc	5	1.5 ± 0.9cc	1.6 cc	0.3–2.8 cc
Duodenum max	V35Gy < 0.5 cc	7	5.7 ± 4.6 cc	5.3 cc	0.4–12.4 cc	Heart/Pericardium	V32Gy ≤ 15 cc	1	0.4 cc	0.4 cc	0.4 cc
Stomach max	V33Gy < 0.5 cc	6	8.7 ± 14.9 cc	3.7 cc	0.5–38.9 cc	Great vessels, non- adjacent wall	V47Gy < 10 cc	0	NA	NA	NA
Small bowel max	V30Gy ≤ 0.5 cc	2	1.6 ± 0.4 cc	1.57 cc	1.26–1.88 cc						
Large bowel max	V35Gy ≤ 0.5 cc	2	0.2 ± 0.3 cc	0.24 cc	0.04–0.44cc	Trachea and ipsilateral bronchus, non-adjacent wall	V10Gy < 0.2 cc	6	0.5 ± 0.4cc	0.4 cc	0.08–1.05 cc
Cord	V25Gy < 0.5cc	0	NA	NA	NA						
Kidney (combined)	Mean < 18 Gy	0	NA	NA	NA	Cord	V8Gy < 1 cc	0	NA	NA	NA